IEEE Robotics and Automation Letters (RAL) paper presented at the
2020 IEEE/RSJ International Conference on Intelligent Robots and Systems (IROS)
October 25-29, 2020, Las Vegas, NV, USA (Virtual)

A Supernumerary Robotic Leg Powered by Magnetorheological Actuators to Assist Human Locomotion

Charles Khazoom[1], Pierre Caillouette[1], Alexandre Girard[1], Jean-Sébastien Plante[1,2]

***Abstract*— Supernumerary robotic limbs are emerging to augment human function. Unlike exoskeletons, these robots provide additional kinematic structures to the user that enable novel human-robot interactions. To assist walking, a supernumerary leg should be compliant to impacts, minimize efforts on users, move quickly when swinging and exert large assistive forces on the ground. Here, we study the potential of a supernumerary leg powered by delocalized magnetorheological clutches (MR leg) to assist walking with three different gaits. Simulations show that the MR leg's low actuation inertia reduces the impact impulse by a factor 4 compared to geared motors and that delocalizing the clutches reduces by half the inertial forces transmitted to the user during swing. An impedance controller receives a reference trajectory based on each ankle's position to move the MR leg in synchrony with the gait cycle. Experiments show that the MR leg can comfortably contact the ground and swing at 3.9 m/s for a 1.4 m/s walk. The MR leg tracks the ankle within 5% of the gait cycle for the leader-follower gait, alternately tracks both ankles for the double gait and contacts the ground in between each step for the three-legged gait. A theoretical upper limit suggests that the average transmitted power in a gait cycle could be 84 W for the leader-follower gait, which is 4 times higher than autonomous ankle exoskeletons.**

I. Introduction

A. Motivation

Supernumerary robotic limbs (SRLs) have recently emerged to assist, augment or restore human functions in various tasks, notably in the fields of manufacturing and rehabilitation. Among others, supernumerary robotic arms have been developed to handle power tools [1], assemble aircraft fuselages [2] or hold objects to free the user's hands [3] and supernumerary fingers can help hemiparetic patients retrieve the lost functions of their weak hand [4]. These multifunctional devices could enable new human-robot behaviors never imagined before, with extra limbs that could adapt to the user's will and needs. For instance, one could walk like a cockroach or a quadruped [5] with extra legs that could also become extra arms in other situations.

SRLs stand out from exoskeletons by enabling humans to perform tasks otherwise unachievable. Exoskeletons provide robotic torques that reduce or replace the biological joint torques for a given task. Lower-limb exoskeletons have been extensively used to reduce the metabolic cost of walking [6] and running [7] and many upper-limb exoskeletons were suggested for stroke rehabilitation [8]. However, since exoskeletons are designed to match the configuration of the biological joints to which they are attached, they can only assist humans in a biomimetic manner and augment or restore already existing functions [9].

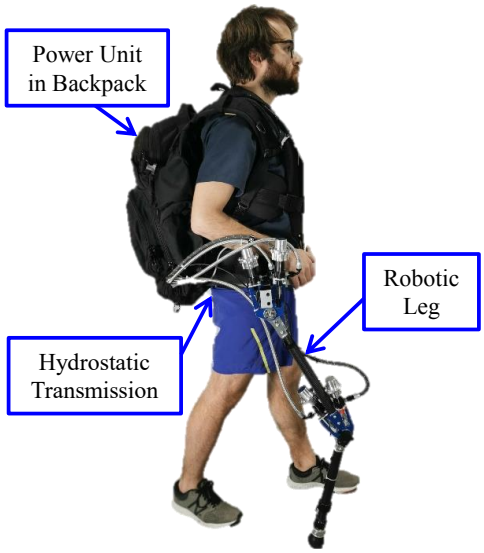

Fig. 1: Picture of a user wearing the MR leg on the right hip with delocalized power units that can be worn in a backpack.

One specific kind of SRL consists of extra wearable robotic legs. These devices add additional kinematic structures that can efficiently synchronize with the human legs to assist locomotion and enable new human-robot gaits.

B. Design Challenges for Supernumerary Robotic Legs

To assist locomotion, a supernumerary leg should have low weight and and low inertia comparable to a human leg in order to minimize the inertial forces transmitted to the user and have low inertia to be compliant to impacts. Also, the robotic leg should be able to move its end-effector as fast as the human foot and still exert high forces on the ground to provide powerful assistance.

Some supernumerary robotic legs have been proposed for specific functions such as supporting the user's carried payload while standing or crawling [10], assisting sit-to-stand motion [9] or prevent falling while walking [9], [11].

In the latter example, the positions of the robotic legs are modulated with respect to the walking gait cycle in order to maximize the user's base of support. Most SRLs have focused on torque density [2], [3] and used slow highly geared motors in a one-per-joint arrangement. This approach

*This work was supported by Canada Research Chairs, the Canadian Space Agency, Exonetik, FRQNT, NSERC and MESI.

[1]Faculty of Engineering, Interdisciplinary Institute for Technological Innovation (3IT), 3000 boul. de l'Université, Sherbrooke, Québec (Canada) J1K 0A5, {Charles.Khazoom, Pierre.Caillouette, Alexandre.Girard2, Jean-Sebastien.Plante}@USherbrooke.ca

[2]Exonetik, 3500 boul. industriel, Sherbrooke, js.plante@exonetik.com

limited possible walking speeds to 0.45 m/s [11] and the resulting lack of back-drivability made the successive ground contact impulses uncomfortable to users [9]. Additionally, geared motors placed on robot joints increase inertia and thus perturbation forces transmitted to the user under high accelerations (e.g. when the leg is swinging). The authors suggest the use of a lighter, faster and more compliant pneumatic actuator, but this technology requires voluminous air tanks and a compressor to be autonomous and suffers from limited force bandwidth [9].

Series elastic actuators have been used to add compliance for prostheses and exoskeletons designed for walking [12], [13], but still require slow highly geared motors to be portable [14], suffer from low force bandwidth and are not back-drivable without control compensation [15].

Optimized, torque-dense motors with a low gear ratio can mitigate impacts through back-drivability, achieve high-bandwidth force control and high torque density [15]. This approach was successful for mobile legged robots [15], exoskeletons [16] and prostheses [17], but can suffer from low efficiency when operating at low speeds [15] and still requires one motor per degree of freedom.

Magnetorheological (MR) actuators are promising to interact with humans in various applications [18], [19]. Their working principle consists of maintaining a clutch driven by a geared motor under continuous slippage. The MR clutch contains an MR fluid that transmits a torque that can be modulated by controlling the magnetic field's strength. This approach decouples the inertia of the geared motor from the actuated output and thus yields high-bandwidth ($\sim$18-25 Hz [1], [20]), fast, torque-dense and back-drivable actuators. Additionally, several MR clutches can be driven by a single motor, which can further increase the torque density for systems with multiple degrees of freedom. MR actuators also eliminate undesired non-linearities inherent to traditional geared electrical motors such as cogging, backlash and stick-slip behaviour due to dry friction. Plus, the MR fluid's viscosity provides MR actuators with linear damping properties that grants increased stability, even in the presence of high controller gains [21]. While the increased damping could possibly reduce energy efficiency, the losses can be minimized by properly controlling the motor's input speed [22]. In all, MR actuators are well-suited to interact with both humans and the external environment, where high compliance, high force, high speed and low inertia are required without adversely affecting force quality.

These benefits come at the expense of slightly added mass from the MR clutches [18], which can be mitigated with a hydrostatic transmission [23] that delocalizes the power unit (containing the MR clutches and the driving motor) away from the robot's joints. This approach has been successfully used for a portable (6.2 kg) and back-drivable ankle exoskeleton that reduced metabolic cost of walking and that delivered 90 N·m per ankle at 1.4 kW within 19 ms while jumping [18] as well as for a fast and powerful multifunctional supernumerary robotic arm [1], [20].

C. Approach

This paper studies the potential of a lightweight, compliant and powerful supernumerary robotic leg powered by delocalized MR actuators (MR leg, Fig. 1) to assist various human-robot gaits in synchrony with the gait cycle. The advantages of the MR leg's low inertia are shown and leveraged to explore three human-robot gaits: the leader-follower gait, the double gait and the three-legged gait. These gaits are demonstrated on a human subject walking on a treadmill.

Section II describes the MR leg design, that can potentially provide 649 N at high speed. It is shown that low actuation inertia reduces the ground impact impulses and that the delocalized architecture reduces the inertial force transmitted to the user. Section III explains the control strategy used to generate and assist the three proposed human-robot gaits. Section IV details the experimental setup. Section V presents the experimental results. These results show that the MR leg can reach end-effector speeds of 3.9 m/s and smoothly contact the ground, which enables the leg to produce the kinematics of the three proposed human-robot gaits. Section VI discusses the perspectives on the assistive capabilities of MR legs and suggest a theoretical maximal average power of 84 W transmitted to the user within the gait cycle while walking at 1.4 m/s.

II. MR Leg Design

A. Overview

The MR leg is a 2.7 kg robotic planar manipulator with two degrees of freedom (Fig. 1 and 2). Although initially built for supernumerary arm applications [20], the design addresses the requirements described in section I-B. These requirements are : 1) mass and sagittal moment of inertia about the hip comparable to a human leg ($\sim$14 kg and 1.2 kg·m^2 for a 75 kg male [24]); 2) high compliance due to the low robotic limb and actuation inertias; 3) high speed (peak of 3.5 m/s relative to the hip for a 1.4 m/s walk during swing phase [25]) and 4) high forces on the ground (666 N in [11]).

The leg is made with lightweight carbon fiber tubes that minimize the mass and inertia of the MR leg. The length of the lower segment can be adjusted for each user to exploit the singularity and apply the largest assistive force possible on the ground. A soft rubber end-effector ensures that the coefficient of friction is high to avoid slippage on the ground.

Each joint is remotely actuated by a power unit delocalized by a hydrostatic antagonist transmission (Fig. 2). The power units' design was detailed in anterior work [1]. The two power units weigh 3.5 kg each and can be worn in a backpack. The total mass of the robot is 9.7 kg, which is lower than the 13.9 kg for a human leg (requirement 1).

Each power unit consists in a high-speed BLDC motor (KDE600XF-1100-G3, KDE Direct, 5.5 kW) and a timing belt (ratio 4.86:1) that drives the input of two MR clutches (Fig. 2). Each clutch (one for each direction) weighs 700 g and modulates the torque on a ball screw on which a ball nut pressurizes a master cylinder (Fig. 2). The pressure is

transmitted to lightweight slave cylinders (270 g each) placed on the robot's joints through a hydrostatic hose containing water. Water was chosen for its convenience and accessibility. The slave cylinders pull on a cable attached to a pulley placed on each joint to generate a torque (Fig. 2). All cylinders are custom and use low-friction rolling diaphragms.

With the MR clutches' design (2 N·m for an input current of 4.5 A), the leads of the ball screws (5 mm and 8 mm for joints B and C, respectively) and pulley radii (22 cm and 14 cm for joints B and C), joint B can apply a maximal continuous torque of ± 55 N·m with a range of motion between $160°$ and $220°$ and joint C, ± 22 N·m with a range between $-90°$ and $10°$. The sign convention is shown on Fig. 3a. The overall ratios from motors to joints are 134:1 and 53:1 for joints B and C respectively, but only 28:1 and 11:1 from the clutches' outputs to the joints.

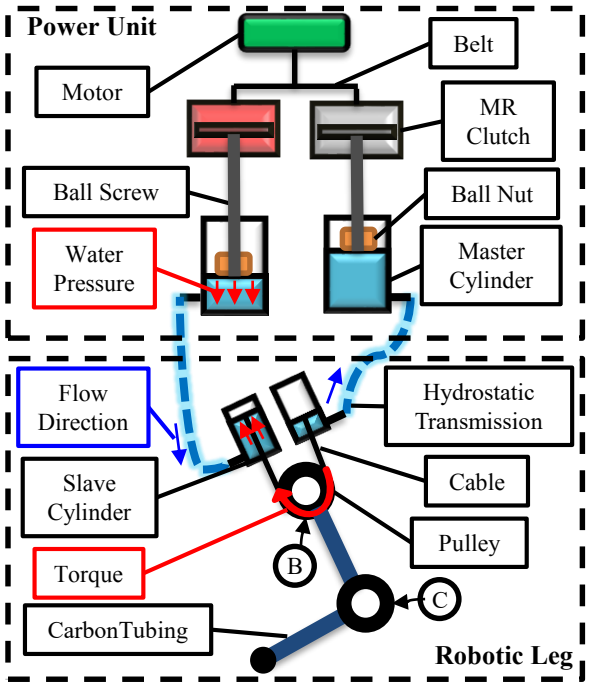

Fig. 2: Schematics of the MR leg, composed of delocalized power units and of a wearable robotic leg joined together by a hydrostatic transmission. Red arrows indicate the water pressure and torque resulting from the activated MR clutch (highlighted in red). Blue arrows indicate flow direction.

B. Speed and Force Capabilities

With the maximal torques of -55 N·m and $+22$ N·m with a configuration close to the singularity ($q_{\mathrm{A}} = 190°$ and $q_{\mathrm{B}} = -20°$) and with the segment lengths of 44.8 cm and 42 cm, the MR leg can exert a force of 649 N on the ground, which is in line with the force requirement of 666 N.

Additionally, the power-dense motor driving the clutches has a maximal speed of ~20000 RPM, corresponding to a theoretical maximal end-effector speed of 30 m/s, which is faster than the speed requirement of 3.5 m/s.

Additionally, the MR leg has a high force bandwidth (18-25 Hz as shown in previous works [1], [20]) and a high power density [18], [19]. In all, these qualities are necessary to gently interact with humans and still generate high assistive forces at high speeds [18].

C. Effect of Mass Delocalization and Actuation Inertia

The MR leg's equivalent inertia about joint B of 1.1 kg·m^2 (including both robotic limb and reflected actuation inertias) compares favorably to that of a human leg (requirement 1). The reasons for such low inertia and the related benefits are twofold. First, the MR clutches reduce the reflected actuation inertia at the joints and thus allow for highly compliant interactions with the ground, effectively reducing the ground contact impulses. Second, the hydrostatic transmission delocalizes the mass of the actuators away from the rapidly moving leg segments. This reduces the inertial forces transmitted to the user when the MR leg accelerates (e.g. during swing) and also contributes to compliance.

A reduced-order dynamical model is developed to quantify the relative benefits of low actuation inertia and actuator delocalization for a supernumerary leg. The model is used to compute the ground contact impulse and the inertial force/torque transmitted to the user when the MR leg swings. Three design cases are compared: a supernumerary leg with 1) delocalized MR clutches – our proposed design (fig. 2); 2) geared motors delocalized by the hydrostatic transmission; and 3) MR clutches and driving motor localized on the robot's joints, without hydrostatic transmission.

1) Dynamical Model: The model developed hereafter is used to compute the ground contact impulse $\boldsymbol{p}$ [15] and the maximal inertial force/torque transmitted to the user.

The model is composed of two rigid bodies attached to the human, who is modelled as a floating particle fixed at point O (Fig. 3a). The system's dynamics is described by (1).

$$\underbrace{\begin{bmatrix} \boldsymbol{H}_{\mathrm{pp}} & \boldsymbol{H}_{\mathrm{pj}} \\ \boldsymbol{H}_{\mathrm{jp}} & \boldsymbol{H}_{\mathrm{jj}} \end{bmatrix}}_{\boldsymbol{H}} \begin{bmatrix} \ddot{\boldsymbol{q}}_{\mathrm{p}} \\ \ddot{\boldsymbol{q}}_{\mathrm{j}} \end{bmatrix} + \boldsymbol{c}(\boldsymbol{q}, \dot{\boldsymbol{q}}) = \boldsymbol{\tau} + \boldsymbol{J}_{\mathrm{c}}^{T} \boldsymbol{f}_{\mathrm{c}}. \qquad (1)$$

The generalized coordinates $\boldsymbol{q} = [\boldsymbol{q}_{\mathrm{p}}\ \boldsymbol{q}_{\mathrm{j}}]^T$ include the position of the base particle $\boldsymbol{q}_{\mathrm{p}} \in \mathbb{R}^2$ and the orientation of the leg $\boldsymbol{q}_{\mathrm{j}} \in \mathbb{R}^2$. The matrix $\boldsymbol{J}_{\mathrm{c}}$ is the Jacobian of the contact constraint, which is chosen as the vertical position of the end-effector staying at ground level after impact. The force $\boldsymbol{f}_{\mathrm{c}}$ is the constraint force, $\boldsymbol{\tau}$ is a vector of generalized forces and $\boldsymbol{c}(\boldsymbol{q}, \dot{\boldsymbol{q}})$ includes Coriolis and gravitational forces. The joint inertia matrix $\boldsymbol{H}_{\mathrm{jj(2x2)}}$ includes both the inertia terms related to the leg's rigid body segments ($\boldsymbol{H}_{\mathrm{rb(2x2)}}$) and the actuators' inertia reflected at the joints (I_{B} and I_{C}):

$$\boldsymbol{H}_{\mathrm{jj}} = \boldsymbol{H}_{\mathrm{rb}} + \mathbf{diag}\,(I_{\mathrm{B}}, I_{\mathrm{C}}) \qquad (2)$$

In (2), the mass delocalization only affects the $\boldsymbol{H}_{\mathrm{rb}}$ matrix. The actuators' rotational inertia reflected on the robot's joints (I_{B} and I_{C}) are greatly influenced by the actuator choice and scale with the gear ratio squared.

The impulse $\boldsymbol{p}$ of the force $\boldsymbol{f}_{\mathrm{c}}$ over the infinitesimal duration of impact (assumed purely inelastic) is computed by integrating (1), yielding

$$\boldsymbol{p} = -\left(\boldsymbol{J}_{\mathrm{c}} \boldsymbol{H}^{-1} \boldsymbol{J}_{\mathrm{c}}^{T}\right)^{-1} \boldsymbol{J}_{\mathrm{c}} \dot{\boldsymbol{q}}^{-} \qquad (3)$$

where $\dot{\boldsymbol{q}}^-$ is the velocity just before the impact [15]. In (3), non-impulsive forces $\boldsymbol{c}(\boldsymbol{q}, \dot{\boldsymbol{q}})$ and $\boldsymbol{\tau}$ do not contribute to $\boldsymbol{p}$ over the infinitesimal impact duration.

To compute the inertial force transmitted to the user's hip (point O, fig. 3) when the robotic leg swings, the acceleration of the center of mass is computed to apply Newton's Second Law, with $\boldsymbol{f}_c = 0$. The torque applied on the user's hip by joint B can be computed from inverse dynamics by using known kinematics with (1). Gravity is neglected in order to capture only the rapidly varying inertial forces, which are the most susceptible to disturb the user.

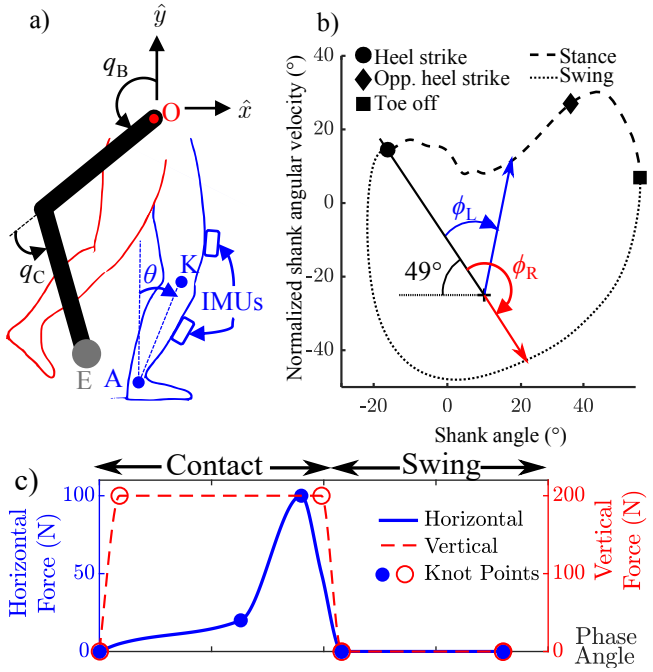

Fig. 3: a) MR leg's orientations and IMU placement. b) The gait cycle is parameterized by the shanks' phase angles ϕ_L and ϕ_R in the phase plane. c) Command $\boldsymbol{F}_{gnd}$ vs phase angle maps with adjustable knot points [18].

2) Numerical Application: Experimental kinematic data from both the user and the MR leg when walking with the leader-follower gait (see later in sections III and IV) were used to compute the impact impulse with (3) and the inertial force/torque transmitted to the user when the MR leg swings with (1). The latter were evaluated for the three design cases.

For our design with delocalized MR clutches, the actual MR leg's geometrical and inertial parameters are used for the $\boldsymbol{H}_{rb}$ matrix, with only the slave cylinders' mass on each joint. The I_B and I_C terms in (2) include the inertias of the MR clutch's output, the ball screws and the water in the hydrostatic transmission, all reflected at the joints [23].

For the delocalized geared motor, I_B and I_C encounter a 22-fold and 33-fold increase due to the addition of the motor's inertia (0.925 kg·cm^2) multiplied by the ratio from motor to joint squared. The $\boldsymbol{H}_{rb}$ matrix is identical to the design case with delocalized MR clutches since mass distribution on the robotic leg is assumed to be the same.

For the localized MR clutches, removing the hydrostatic transmission reduces I_B and I_C, but the $\boldsymbol{H}_{rb}$ matrix is modified because of the added mass of 1.3 kg on each of the robot's joints. For all three cases, the mass of the floating base particle is set to 20 kg (1/3 of the user's mass). Although this value is uncertain and depends on how much of the user's weight is born by the MR leg, the impulse results and related conclusions are not sensitive to this value.

The vertical impact impulse on the end-effector and the maximal inertial force and torque magnitudes during swing for the three design cases are shown in Table I.

TABLE I: Effect of delocalization and actuation inertia on impact impulse and inertial efforts transmitted to the user.

	Impact	**Swing**	
Design	***Impulse (N·s)***	***Inertial force magnitude (N)***	***Inertial torque (N·m)***
Delocalized MR clutches	0.37	28	12.35
Delocalized geared motor	1.44	28	12.35
Localized MR clutches	0.57	51	21.59

The delocalization of the MR clutches' mass away from the MR leg's joints reduces the impact impulse by a factor 1.5 (localized vs delocalized MR clutches). However, reducing the actuation inertia by inserting MR clutches in the transmission reduces this vertical impulse even more, by a factor 4 (delocalized geared motors vs delocalized MR clutches). Thus, the low actuation inertia intrinsic to MR actuators contributes much more to the MR leg's compliance to impacts than the reduced mass on the joints.

Additionally, the maximal inertial force transmitted to the user when the MR leg swings is reduced by a factor 1.8 when delocalizing the MR actuators. Similarly, the maximal torque magnitude transmitted to the user is reduced by a factor 1.7. The inertial force and torque magnitudes are identical for the two delocalized design cases, since the mass distribution on the leg is assumed identical.

III. MR Leg Control

The MR leg's controller is designed to apply a varying force on the ground and swing back into position for the next cycle. This is achieved by using a reference generator that feeds the end-effector's reference position to an impedance controller and that generates open-loop torque commands to push on the ground in synchrony with the walking gait cycle (Fig. 4). The reference generator and the impedance controller are described hereafter.

A. Reference Generator

1) User Measurements: The reference generator uses measurements from four inertial measurement units (IMUs) to generate the MR leg's reference position, which is modulated according to one of the three proposed gaits (Fig. 4) in synchrony with the gait cycle. The IMUs are worn on the left and right thighs and shanks and measure the limbs' orientations $\boldsymbol{\theta}_i \in \mathbb{R}^2$ and angular rates $\dot{\boldsymbol{\theta}}_i$ in the sagittal plane (Fig. 3a). The subscripts i = L, R correspond to the left and right sides respectively and each vector $\boldsymbol{\theta}_i$ include the orientations of the thigh and shank from a given side.

The orientations are used along with the lengths of the thighs and shanks to compute the positions $\boldsymbol{r}^{A_L/O}$ and

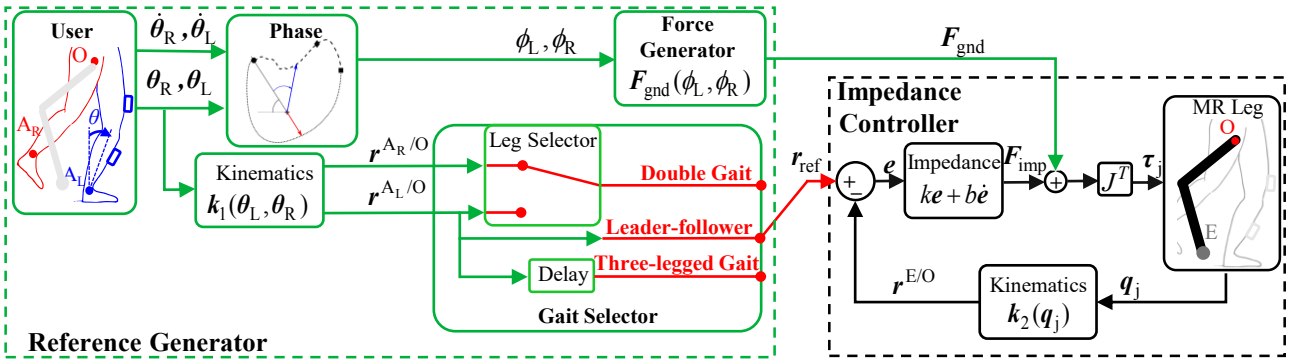

Fig. 4: The controller is composed of a reference generator that feeds the reference trajectory and an open-loop force command to an impedance controller.

$\boldsymbol{r}^{\mathrm{A_R/O}}$ of each ankle ($\mathrm{A_L}$ and $\mathrm{A_R}$). This is achieved by using the forward kinematics function $\boldsymbol{k}_1$ (Fig. 4).

2) Gait Selector: In this paper, three different human-robot gaits are presented. To change the characteristics of the gait, the reference position is calculated differently by the gait selector (Fig. 4). For the leader-follower gait, the position $\boldsymbol{r}^{\mathrm{A_L/O}}$ is fed directly into the impedance controller, where the MR leg worn on the right side tracks the position of the opposite left ankle during the whole gait cycle. For the double gait, the leg selector (Fig. 4) is designed to track each leg alternately and assist push-off at each step, twice per cycle. The leg selector switches to the aftmost leg according to the variable s, given by

$$s = \mathrm{sign}\left[\left(\boldsymbol{r}^{\mathrm{A_L/O}} - \boldsymbol{r}^{\mathrm{A_R/O}}\right)\cdot\hat{\boldsymbol{x}}\right], \tag{4}$$

with $\hat{x}$ a unit vector in the anteroposterior direction (Fig. 3a).

In the three-legged gait, the reference position corresponds to the left leg's trajectory delayed three-quarter of a step period. This yields a three-legged gait where the MR leg takes a step in between the steps of the two biological legs.

3) Force Generator: The force generator feeds an open-loop force command $\boldsymbol{F}_{\mathrm{gnd}}$ to the impedance controller in order to modulate the assistive force $\boldsymbol{f}_{\mathrm{c}}$ applied by the ground in synchrony with the human gait, which is parameterized by the shanks' phase angle ϕ_i (Fig. 3b). The latter is a time-independent parameter that well estimates the walking gait cycle for steady and transient walking [18] and is computed from the measured shanks' angles and angular velocities (Fig. 3b). Adjustable $\boldsymbol{F}_{\mathrm{gnd}}$ vs ϕ_i profiles can be used to modulate the horizontal and vertical components of the force when the MR leg touches the ground and apply zero force when the MR leg swings (Fig. 3c). The components of $\boldsymbol{F}_{\mathrm{gnd}}$ can be adjusted to enforce the no-slip constraint at contact while propelling the body forwards at push-off (Fig. 3c).

B. Impedance Controller

The impedance controller (Fig. 4) ensures that the MR leg's end-effector tracks the reference generator's trajectories while ensuring compliant interactions with the user and with the ground. The end-effector's position relative to the hip ($\boldsymbol{r}^{\mathrm{E/O}}$) is computed with the forward kinematics function $\boldsymbol{k}_2$, that uses the lengths of the MR leg's segments and their orientations $\boldsymbol{q}_{\mathrm{j}} = [q_{\mathrm{B}}\ q_{\mathrm{C}}]^T$, as defined in Fig. 3a. The joint torques $\boldsymbol{\tau}_{\mathrm{j}}$ to achieve the total force from both the impedance and the force generator are computed by using $\boldsymbol{J}^T$, where $\boldsymbol{J}$ is the Jacobian of $\boldsymbol{r}^{\mathrm{E/O}}(q_{\mathrm{B}}, q_{\mathrm{C}})$ (Fig. 3a). The clutch input current is commanded in open loop from a known relationship between $\boldsymbol{\tau}_{\mathrm{j}}$ and current, derived experimentally.

IV. Experimental Setup

A. System Implementation

The IMUs' orientations and angular velocities (SEN-14001, SparkFun) are acquired and processed by a Robot Operating System program running on a desktop computer to compute the ankles' positions. These positions are sent via a RS-232 serial interface to a real-time target computer (Performance real-time target machine, Speedgoat).

The gait selector and the impedance controller are implemented at 1 kHz on the target machine, which controls the MR clutches input current with two servo drives per joints (AMC30A8, Advanced Motion Controls) and acquires the measurements of the load-cell placed at the end-effector (Mini45, ATI ; not used for control) and the encoders placed on the robot's joints (E5-5000-315-IE-S-D-G-1, US Digital). For the current stage of development, the control electronics, electrical power supply and power units are tethered.

B. Testing Protocol

For this proof-of-concept study, trials with a single subject were judged sufficient to assess the MR leg's performance (intrinsic to its design) and demonstrate the feasibility of the human-robot gaits with the MR leg. The leader-follower gait, the double gait and the three-legged gait (Fig. 4) were implemented without the force generator (Fig. 4) on an inexperienced single male subject (60 kg, 1.70 m). Preliminary trials were necessary to adjust the MR leg's length and controller to the particular subject's gait. After these adjustments, the subject was asked to accelerate from rest up to 1.4 m/s on the treadmill, walk for 30 s and decelerate until the treadmill comes to a complete rest for each gait. The protocol was approved by the Comité d'éthique de la recherche du CIUSSS de l'Estrie. The subject was healthy and gave informed consent after potential risks and consequences of the experiment were explained.

C. Data Analysis and Processing

The tracking delay between the horizontal reference trajectory and the end-effector's horizontal position with respect to

the hip was evaluated. The number of shifted samples at the maximal cross-correlation between both signals was used. The results from these analyses are presented in section V.

To evaluate the theoretical assistive capabilities of the MR leg when walking with the leader-follower gait, the maximal available force $\boldsymbol{f}_c$ as the MR leg changes its configuration during contact was computed. The maximal joint torques (-55 N·m for joint B and $+21.2$ N·m for joint C) and the measured kinematics from the user and the MR leg were used along with (1). The MR leg's power was computed by multiplying the applied torques by the joints' angular velocities. The total energy transmitted to the user during stance was computed as the integral of the total power with respect to time, from 0 to 60% of the gait cycle. These extrapolated results are presented in section VI.

V. Experimental Results

The three human-robot gaits are demonstrated in the attached video, where the user walks at 1.4 m/s with the MR leg moving in synchrony with the gait cycle. The MR leg smoothly meets the ground and swings back in front in preparation for the next step without disturbing the user.

While walking with the leader-follower gait, the MR leg tracks the left ankle's position right from the first step with the ankle and end-effector reaching a maximal speed of 3.4 m/s (Fig. 5). The MR leg's position slightly lags behind its reference position. The time difference at the maximal cross-correlation between the reference and the end-effector position's is 50 ms. With the period of 1.0 s, this error, corresponding to 5% of the gait cycle, was not perceived by the user and was consistent across all steps.

The MR leg's peak impact force on the treadmill is 70 N with the impedance control powered on. This force did not impede the user's ability to walk comfortably with the MR leg, which demonstrates sufficient compliance to impacts. This compliance, combined with the compliant impedance controller, is also favorable to interact with humans in unpredictable environments since it allows the robot to meet obstacles without breaking or hurting the user.

For the double gait, the MR leg tracks the aftmost leg and thus alternates between the user's left and right leg to assist all steps (Fig. 6). Switching between the legs occurs when the ankles' horizontal positions become equal, as one leg swings back in front while the other stance leg starts to trail behind in preparation for push-off. Upon switching, the MR leg's horizontal velocity rapidly decreases from $\sim$2 m/s to ~ -1.4 m/s (Fig. 6b). Similarly to the leader-follower gait, the delay of 7% of the gait cycle was consistent and comfortable to the user.

As for the three-legged gait, the end-effector tracks a time-delayed version of the left ankle's position relative to the hip (Fig. 7a). This time delay was adjusted to ensure that the end-effector meets the ground between two successive right and left biological feet while walking at 1.4 m/s. With this gait, a complete cycle of period T consists of the right leg first contacting the ground at time $t = 0$, followed by the MR leg at time $T/4$, by the left ankle at $T/2$ and by the

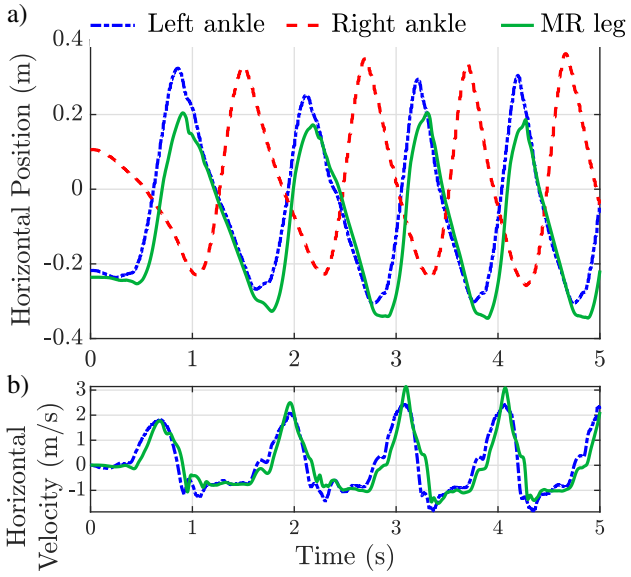

Fig. 5: MR leg and ankle horizontal kinematics for the leader-follower gait while accelerating from rest up to 1.4 m/s. a) Position of the left and right ankles and of the MR leg's end-effector relative to the hip. b) Left ankle and end-effector velocity.

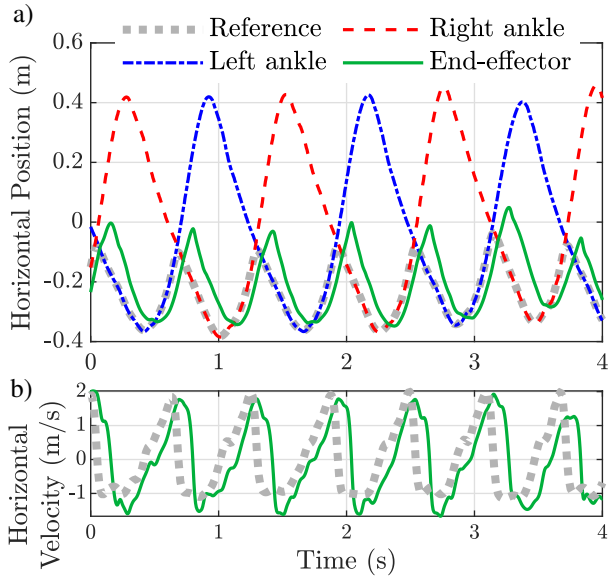

Fig. 6: MR leg and ankle horizontal kinematics for the double gait with the end-effector following the aftmost ankle. a) Position of the ankles and the end-effector relative to the hip. b) Reference and end-effector velocity.

right leg completing the cycle when contacting the ground at time $t = T$. This pattern is shown on Fig. 7a, where the MR leg's end-effector successively reaches the foremost horizontal position relative to the hip 0.23 s after the right leg and 0.24 s before the left leg in average, as determined by the maximal cross-correlation. The slight difference between the two user's legs corresponds to $\sim$1% of the gait cycle.

The MR leg reaches a maximal speed of 3.9 m/s (Fig. 7b). This speed corresponds to less than 15% of the motor's available speed, suggesting that the MR leg can assist faster movements such as running or prevent falls by swinging the MR leg faster than the biological legs can.

This three-legged gait strategy could be used in combi-

nation with a second MR leg that would follow a delayed version of the right leg's trajectory to yield a human-robot quadruped gait that would synchronize with the user's natural bipedal gait like suggested by Gonzalez [5].

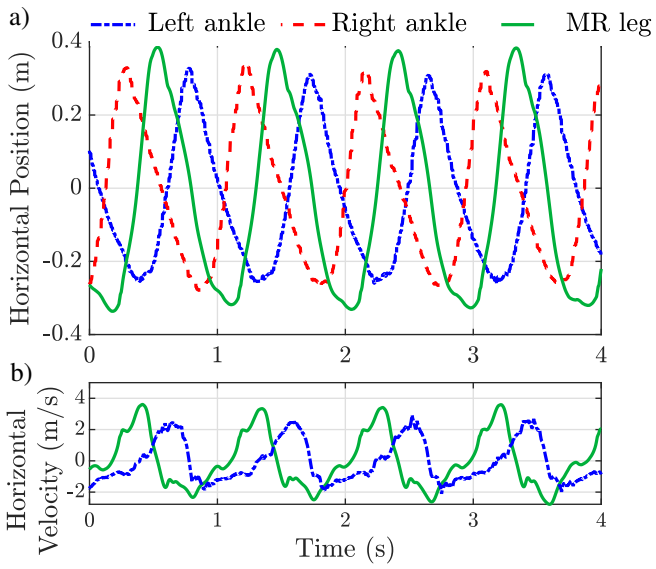

Fig. 7: MR leg and ankle horizontal kinematics for the three-legged gait. a) Position of the ankles and the end-effector relative to the hip. The end-effector reaches the foremost position between the right and left ankles. b) Left ankle and end-effector velocity.

VI. Perspectives on the Assistive Capabilities of MR Legs

With the feasibility of the human-robot gaits with the MR leg now demonstrated experimentally under low force conditions, maximal force and power predictions from the model (1) are now superimposed on the experimentally measured kinematics to provide a first bounding estimate of the MR leg's potential as an assistive device for walking. Note that the force levels presented come from the robot used in this paper, which was initially designed as a supernumerary arm and has yet to be optimized for leg applications.

Maximal theoretical available force and power as a function of the left leg's gait cycle when walking with the leader-follower gait are shown on Fig. 8 for the stance phase (0 to 60% of the gait cycle). The horizontal force component is small at the beginning of the gait cycle, but increases up to 196 N at the end of the stance phase. The vertical component ranges between 241 N and 346 N, which implies that the MR leg could support between 40% and 58% of the user's weight throughout stance phase. With the treadmill speed set at 1.4 m/s, the MR leg's power peaks at 119 W and 122 W at 8% and 54% of the gait cycle, respectively.

The ratio of horizontal over vertical force is always smaller than 0.8. Thus the no-slip condition can be respected for coefficients of friction over 0.8.

The increase of the horizontal force component throughout stance is due to the MR leg's being oriented more forwards as the gait advances. This behavior may be beneficial in order to provide proper assistance timing, which has been shown to be important to reduce the metabolic cost of walking with exoskeletons [26], [27]. The occurrence of the second peak of 122 W at 55% of the gait cycle is in line with peak powers of ankle exoskeletons, which occur with similar magnitude at around 52% of the gait cycle [18], [28].

The average power transmitted to the user across the entire gait cycle (Fig. 8) is 84 W. This theoretical transmitted power is almost 4 times higher than the best autonomous bilateral ankle exoskeletons (∼20 W for both legs, [18], [28]), 2.4 times higher than a bilateral multi-joint soft exosuit (∼34 W for both legs [29]) and 1.6 times higher than a powerful tethered ankle exoskeleton (∼53 W for both legs [30]). While these numbers must be considered as a first estimate of an upper bound and are yet to be validated experimentally, it may be possible that MR legs be capable of injecting significantly more energy in the gait cycle than conventional exoskeletons, where the robot's joint angles must be equal to the biological joints' angles and where work can only be done when the biological joints have high angular velocities.

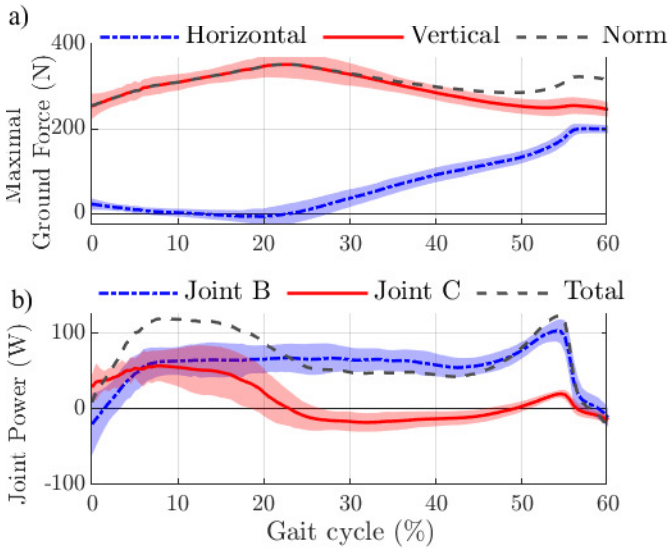

Fig. 8: Theoretical force (a) and power (b) capabilities of the MR leg with the leader-follower gait as a function of the left leg's gait cycle during stance phase, averaged over 32 steps. The shaded areas correspond to ±1 standard deviation across all steps.

Finally, given the multifunctional nature of MR-actuated wearable robots [1], [18], MR legs could serve as a multi-purpose MR limbs that could not only augment or restore human locomotion, but also serve as a fall prevention device or turn into a supernumerary arm [20], [1] or a wearable robotic tail.

VII. Conclusion

This paper studied the potential of a supernumerary leg powered by delocalized MR actuators to assist walking. A dynamical model showed that MR clutches contribute the most to the robot's compliance to impacts and that their delocalization reduces the efforts transmitted to the user when swinging by half.

These properties were demonstrated experimentally and leveraged to explore three new human-robot gaits that require both fast and strong actuation. The end-effector reached

speeds of 3.9 m/s when walking at 1.4 m/s. Given the MR leg's maximal continuous joint torques ($\pm$55 N·m and $\pm$22 N·m), the maximal assistive ground force and power were extrapolated. While they must be carefully validated experimentally, the results suggest that a supernumerary leg may be able to provide positive power throughout the entire ground contact, which contrasts with exoskeleton assistance that can only produce positive mechanical work when the user's biological joints are moving in the same direction as the applied torques.

Future work will focus on discovering the most assistive gait, on properly modulating the ground forces using the force generator and on comparing the metabolic cost of walking with the MR leg on multiple subjects. Assisting even faster movements such as running and reducing the weight of the power units are also envisioned.

REFERENCES

[1] C. Veronneau, J. Denis, L.-P. Lebel, M. Denninger, V. Blanchard, A. Girard, and J.-S. Plante, "Multifunctional Remotely Actuated 3-DOF Supernumerary Robotic Arm Based on Magnetorheological Clutches and Hydrostatic Transmission Lines," *IEEE Robotics and Automation Letters*, pp. 1–1, 2020.

[2] F. Parietti and H. H. Asada, "Supernumerary Robotic Limbs for aircraft fuselage assembly: Body stabilization and guidance by bracing," in *2014 IEEE International Conference on Robotics and Automation (ICRA)*, pp. 1176–1183, May 2014.

[3] B. L. Bonilla and H. H. Asada, "A robot on the shoulder: Coordinated human-wearable robot control using Coloured Petri Nets and Partial Least Squares predictions," in *2014 IEEE International Conference on Robotics and Automation (ICRA)*, pp. 119–125, May 2014.

[4] T. Ort, F. Wu, N. C. Hensel, and H. H. Asada, "Supernumerary Robotic Fingers as a Therapeutic Device for Hemiparetic Patients," in *ASME 2015 Dynamic Systems and Control Conference*, American Society of Mechanical Engineers Digital Collection, Jan. 2016.

[5] D. J. Gonzalez, *Extra Robotic Legs for Augmenting Human Payload and Positioning Capabilities*. Thesis, Massachusetts Institute of Technology, 2019.

[6] L. M. Mooney, E. J. Rouse, and H. M. Herr, "Autonomous exoskeleton reduces metabolic cost of human walking," *Journal of NeuroEngineering and Rehabilitation*, vol. 11, p. 151, Nov. 2014.

[7] G. Lee, J. Kim, F. A. Panizzolo, Y. M. Zhou, L. M. Baker, I. Galiana, P. Malcolm, and C. J. Walsh, "Reducing the metabolic cost of running with a tethered soft exosuit," *Science Robotics*, vol. 2, p. eaan6708, May 2017.

[8] J. D. Sanjuan, A. D. Castillo, M. A. Padilla, M. C. Quintero, E. E. Gutierrez, I. P. Sampayo, J. R. Hernandez, and M. H. Rahman, "Cable driven exoskeleton for upper-limb rehabilitation: A design review," *Robotics and Autonomous Systems*, vol. 126, p. 103445, Apr. 2020.

[9] F. Parietti, *Design and Control of Supernumerary Robotic Limbs*. Thesis, Massachusetts Institute of Technology, 2016.

[10] D. J. Gonzalez and H. H. Asada, "Hybrid Open-Loop Closed-Loop Control of Coupled Human–Robot Balance During Assisted Stance Transition With Extra Robotic Legs," *IEEE Robotics and Automation Letters*, vol. 4, pp. 1676–1683, Apr. 2019.

[11] F. Parietti, K. C. Chan, B. Hunter, and H. H. Asada, "Design and control of Supernumerary Robotic Limbs for balance augmentation," in *2015 IEEE International Conference on Robotics and Automation (ICRA)*, pp. 5010–5017, May 2015.

[12] K. A. Witte, J. Zhang, R. W. Jackson, and S. H. Collins, "Design of two lightweight, high-bandwidth torque-controlled ankle exoskeletons," in *2015 IEEE International Conference on Robotics and Automation (ICRA)*, pp. 1223–1228, May 2015.

[13] A. F. Azocar, L. M. Mooney, L. J. Hargrove, and E. J. Rouse, "Design and Characterization of an Open-Source Robotic Leg Prosthesis," in *2018 7th IEEE International Conference on Biomedical Robotics and Biomechatronics (Biorob)*, pp. 111–118, Aug. 2018.

[14] W. van Dijk, C. Meijneke, and H. van der Kooij, "Evaluation of the Achilles Ankle Exoskeleton," *IEEE Transactions on Neural Systems and Rehabilitation Engineering*, vol. 25, pp. 151–160, Feb. 2017.

[15] P. M. Wensing, A. Wang, S. Seok, D. Otten, J. Lang, and S. Kim, "Proprioceptive Actuator Design in the MIT Cheetah: Impact Mitigation and High-Bandwidth Physical Interaction for Dynamic Legged Robots," *IEEE Transactions on Robotics*, vol. 33, pp. 509–522, June 2017.

[16] G. Lv, H. Zhu, and R. D. Gregg, "On the Design and Control of Highly Backdrivable Lower-Limb Exoskeletons: A Discussion of Past and Ongoing Work," *IEEE Control Systems Magazine*, vol. 38, pp. 88–113, Dec. 2018.

[17] T. Elery, S. Rezazadeh, C. Nesler, J. Doan, H. Zhu, and R. D. Gregg, "Design and Benchtop Validation of a Powered Knee-Ankle Prosthesis with High-Torque, Low-Impedance Actuators," in *2018 IEEE International Conference on Robotics and Automation (ICRA)*, pp. 2788–2795, May 2018.

[18] C. Khazoom, C. Véronneau, J. L. Bigué, J. Grenier, A. Girard, and J. Plante, "Design and Control of a Multifunctional Ankle Exoskeleton Powered by Magnetorheological Actuators to Assist Walking, Jumping, and Landing," *IEEE Robotics and Automation Letters*, vol. 4, pp. 3083–3090, July 2019.

[19] J. Viau, P. Chouinard, J.-P. L. Bigue, G. Julio, F. Michaud, and J.-S. Plante, "Tendon-Driven Manipulator Actuated by Magneto-Rheological Clutches Exhibiting Both High-Power and Soft Motion Capabilities," *IEEE/ASME Transactions on Mechatronics*, 2016.

[20] C. Véronneau, J. Denis, L.-P. Lebel, M. Denninger, J.-S. Plante, and A. Girard, "A Lightweight Force-Controllable Wearable Arm Based on Magnetorheological-Hydrostatic Actuators," in *2019 International Conference on Robotics and Automation (ICRA)*, pp. 4018–4024, May 2019.

[21] D. W. Weir, J. E. Colgate, and M. A. Peshkin, "Measuring and Increasing Z-Width with Active Electrical Damping," in *2008 Symposium on Haptic Interfaces for Virtual Environment and Teleoperator Systems*, pp. 169–175, Mar. 2008.

[22] M.-A. Bégin, *Conception et validation d'un contrôleur optimisant la durée de vie et la consommation énergétique d'un actionneur magnétorhéologique*. PhD thesis, Université de Sherbrooke, 2018.

[23] C. Veronneau, J.-P. Lucking Bigue, A. Lussier-Desbiens, and J.-S. Plante, "A High-Bandwidth Back-Drivable Hydrostatic Power Distribution System for Exoskeletons Based on Magnetorheological Clutches," *IEEE Robotics and Automation Letters*, vol. 3, pp. 2592–2599, July 2018.

[24] P. de Leva, "Adjustments to Zatsiorsky-Seluyanov's segment inertia parameters," *Journal of Biomechanics*, vol. 29, pp. 1223–1230, Sept. 1996.

[25] C. A. Fukuchi, R. K. Fukuchi, and M. Duarte, "A public dataset of overground and treadmill walking kinematics and kinetics in healthy individuals," *PeerJ*, vol. 6, p. e4640, Apr. 2018.

[26] S. Galle, P. Malcolm, S. H. Collins, and D. De Clercq, "Reducing the metabolic cost of walking with an ankle exoskeleton: Interaction between actuation timing and power," *Journal of Neuroengineering and Rehabilitation*, vol. 14, p. 35, Apr. 2017.

[27] Y. Ding, F. A. Panizzolo, C. Siviy, P. Malcolm, I. Galiana, K. G. Holt, and C. J. Walsh, "Effect of timing of hip extension assistance during loaded walking with a soft exosuit," *Journal of NeuroEngineering and Rehabilitation*, vol. 13, p. 87, Oct. 2016.

[28] L. M. Mooney and H. M. Herr, "Biomechanical walking mechanisms underlying the metabolic reduction caused by an autonomous exoskeleton," *Journal of NeuroEngineering and Rehabilitation*, vol. 13, p. 4, Jan. 2016.

[29] Y. Ding, I. Galiana, A. T. Asbeck, S. M. M. D. Rossi, J. Bae, T. R. T. Santos, V. L. de Araujo, S. Lee, K. G. Holt, and C. Walsh, "Biomechanical and Physiological Evaluation of Multi-Joint Assistance With Soft Exosuits," *IEEE Transactions on Neural Systems and Rehabilitation Engineering*, vol. 25, pp. 119–130, Feb. 2017.

[30] J. Zhang, P. Fiers, K. A. Witte, R. W. Jackson, K. L. Poggensee, C. G. Atkeson, and S. H. Collins, "Human-in-the-loop optimization of exoskeleton assistance during walking," *Science (New York, N.Y.)*, vol. 356, pp. 1280–1284, June 2017.